Journal of The Electrochemical Society, **158** (2) A93-A101 (2011)
0013-4651/2010/158(2)/A93/9/$28.00 © The Electrochemical Society

Reduction of an Electrochemistry-Based Li-Ion Battery Model via Quasi-Linearization and Padé Approximation

Joel C. Forman, Saeid Bashash, Jeffrey L. Stein, and Hosam K. Fathy[z]

Mechanical Engineering Department, The University of Michigan, Ann Arbor, Michigan 48109-2125, USA

This paper examines an electrochemistry-based lithium-ion battery model developed by Doyle, Fuller, and Newman. The paper makes this model more tractable and conducive to control design by making two main contributions to the literature. First, we adaptively solve the model's algebraic equations using quasi-linearization. This improves the model's execution speed compared to solving the algebraic equations via optimization. Second, we reduce the model's order by deriving a family of analytic Padé approximations to the model's spherical diffusion equations. The paper carefully compares these Padé approximations to other published methods for reducing spherical diffusion equations. Finally, the paper concludes with battery simulations showing the significant impact of the proposed model reduction approach on the battery model's overall accuracy and simulation speed.
 [DOI: 10.1149/1.3519059]

Manuscript submitted May 21, 2010; revised manuscript received August 29, 2010. Published December 9, 2010; publisher error corrected January 3, 2010.

This paper examines the problem of developing reduced, electrochemistry-based models of the dynamics of charging and discharging of lithium-ion batteries. The overarching goal of the paper is to develop lithium-ion battery models that satisfy two important but potentially conflicting objectives. First, the models must have the ability to accurately predict the performance of lithium-ion batteries in applications involving potentially complex and rapid charge/discharge cycles, e.g., hybrid vehicle applications. Second, the models must run with sufficient speed to enable battery system design, optimization, and control.

Several models have been used to monitor battery state of charge (SOC) and state of health.[1-4] While these models are very desirable for control and estimation, they do not capture all of the high rate dynamics associated with hybrid vehicle drive cycles. For this one can use an electrochemical battery model. One such model is provided by Doyle, Fuller, and Newman, with the addition of a potential degradation mechanism provided by Ramadass et al.[5-8] There are two major numerical difficulties with this electrochemical model. The first is the large number of state variables: a finite difference discretization of the model with M points along the width of the cell and N points in the pseudospherical direction has approximately $(2/3) * M * N$ state variables. The second challenge is the model's nonzero index, represented by approximately $(2/3) * M * N$ algebraic equations, most of them involving a hyperbolic sine nonlinearity. This results in a large set of differential algebraic equations (DAEs). Ideally, one would like a model that: (i) runs quickly with a low number of state variables to enable optimal design and control studies, while (ii) still retaining the ability to accurately model complex, high rate charge/discharge cycles.

Applying model reduction techniques to the above electrochemical battery model can bring it closer to the ideal speed and fidelity goals. Several reductions of this model are already presented in the literature. Some of these reductions pay special attention to the spherical diffusion submodel because it appears repeatedly within the full battery model and contributes significantly to its state variable count. Reduction of the spherical diffusion submodel has been approached in a variety of different ways. Spherical diffusion dynamics have been approximated by parabolic and quartic profiles.[9] These profile approximations are analytic but have not been generalized to higher orders. Proper orthogonal decomposition (POD) and residue grouping (RG) have also been used with great success.[10,11] Both POD and RG are numerical in nature and POD requires, as input, a representative set of battery state trajectories.

In addition to the above studies focusing on spherical diffusion, researchers have also examined the problem of reducing the electrochemistry-based battery model as a whole. The single-particle model and electrode-averaged model have been shown to be excellent at rates up to at least 1C, where "C" is defined as the current needed for fully charging/discharging a battery in 1 h.[4,12] These models have the added advantage of not requiring the solution of large sets of algebraic equations. Proper orthogonal decomposition has been used for reducing the full battery model.[10] This furnishes a reduced model capable of simulating constant high rate charging and discharging. However, the model's performance increase is limited by the need to still solve a large set of algebraic equations. A model reduction based on "volume averaging, approximation methods, and intuition" is presented in Ref. 13, and shown to be computationally efficient for lower charge/discharge rates. The battery model can also be reduced using orthogonal polynomials, which decrease the total number of model equations.[14,15]

This paper contributes to the above literature by providing two additional unique reductions to the above electrochemistry-based battery model. The first contribution is a quasi-linearized model of intercalation current that aids in efficiently solving the battery model's algebraic equations. The second contribution is a family of analytic Padé approximations to spherical diffusion that substantially reduce the number of state variables present in the model while retaining a high level of accuracy.

The remainder of the paper introduces and discusses the full battery model, then shows how to efficiently solve the model's algebraic equations via quasi-linearization and how to reduce its order substantially through a family of Padé approximations of the spherical diffusion equation. The paper then compares the Padé approximations to other methods used in the model reduction of spherical diffusion. Finally, the paper presents numerical simulations of the reduced battery model, and provides some conclusions.

The Lithium-Ion Battery Model

This section summarizes the lithium-ion battery model originally developed by Doyle, Fuller, and Newman. The section also summarizes the degradation submodel contributed to this battery model by Ramadass et al.[5-7,12] This submodel represents the dynamics of anode-side resistive film formation, a process that may have significant impact on long-term battery health for certain battery chemistries.[7,12,16] The literature describes several other lithium-ion battery aging mechanisms, including dendrite formation, carbon dissolution, electrolyte degradation, and electrode structure distortion.[16,17] We present the degradation equations by Ramadass et al. here in order to show how one can incorporate them into this paper's proposed quasi-linearization methods. The quasi-linearization and Padé approximation methods presented in this paper are equally applicable to the original model by Doyle, Fuller, and Newman without this degradation submodel.

The diffusion of Li-ions within the electrolyte is governed by Fick's law of linear diffusion combined with an intercalation current density term, J, transferring Li-ions between the solution and solid

[z] Corresponding Author E-mail: hfathy@umich.edu

$$\varepsilon_2 \frac{\partial c_2}{\partial t} = \nabla \cdot (D_2^{\text{eff}} \nabla c_2) + \frac{1 - t^+}{F} J \quad [1]$$

The above intercalation current density, J, also acts as an input to the dynamics of Li-ion diffusion within the solid. This diffusion occurs at every point in the anode and cathode and can be modeled using a spherical, radially symmetric diffusion law as follows

$$\frac{\partial c_{1,j}}{\partial t} = \frac{D_{1,j}}{r^2} \frac{\partial}{\partial r}\left(r^2 \frac{\partial c_{1,j}}{\partial r} \right) \quad [2]$$

The intercalation current density, J, consists of two components. The first component is a main intercalation reaction current density, J_1, and the second component is the side intercalation current density, J_{sd}. The main intercalation current density is driven predominantly by potential differences between the solid and electrolyte solution, and governed by the well-known Butler–Volmer equation

$$J_1 = a_j i_{0,j} \left[\exp\left(\frac{\alpha_{a,j} F}{\bar{R} T} \eta_j \right) - \exp\left(- \frac{\alpha_{c,j} F}{\bar{R} T} \eta_j \right) \right] \quad [3]$$

$$i_{0,j} = k_j (c_{1,j}^{\max} - c_{1,j}^S)^{\alpha_{a,j}} (c_{1,j}^S)^{\alpha_{c,j}} (c_2)^{\alpha_{a,j}}, \quad j = n,p \quad [4]$$

The overpotentials in the above equations equal the difference between the solid and solution potentials minus the reference potentials for the main intercalation reaction, which in turn depend on the local state of charge. In other words, the overpotentials are given by

$$\eta_{\text{p}} = \phi_1 - \phi_2 - U_{\text{ref,p}} \quad [5]$$

$$\eta_{\text{n}} = \phi_1 - \phi_2 - U_{\text{ref,n}} - \frac{J}{a_{\text{n}}} R_{\text{film}} \quad [6]$$

Because the above potentials/overpotentials can change much faster than the Li-ion concentrations, they are typically assumed to respond instantaneously. This assumption is valid to approximately 100 Hz.[18] The solid potential is governed by Ohm's law with a term governing the charge transfer due to intercalation

$$\nabla \cdot (\sigma_j^{\text{eff}} \nabla \phi_{1,j}) - J = 0 \quad [7]$$

Similarly, the solution potential is governed by Ohm's law, intercalation current density, and the charge carried by the ions in solution

$$\nabla \cdot (\kappa^{\text{eff}} \nabla \phi_2) + J + \nabla \cdot (\kappa_{\text{D}} \nabla \ln(c_2)) = 0 \quad [8]$$

The above system of equations governs the dynamics of charging and discharging in the Li-ion cell. From a dynamic systems perspective it is a system of differential algebraic equations, where the differential equations govern the diffusion dynamics and the algebraic equations constrain the potentials and intercalation current accordingly. A degradation component can be added to this model by assuming that film growth in the anode is governed by an electrochemically driven irreversible side reaction. This side reaction is itself governed by a side reaction overpotential as follows

$$\eta_{\text{sd}} = \phi_1 - \phi_2 - U_{\text{ref,sd}} - \frac{J}{a_{\text{n}}} R_{\text{film}} \quad [9]$$

$$J_{\text{sd}} = - i_{0,\text{sd}} a_{\text{n}} \exp\left(- \frac{\alpha_{c,n} F}{\bar{R} T} \eta_{\text{sd}} \right) \quad [10]$$

The above side reaction creates a resistive film at a rate proportional to the side reaction current density, i.e.

$$\frac{\partial \delta_{\text{film}}}{\partial t} = - \frac{J_{\text{sd}} M_{\text{p}}}{a_{\text{n}} \rho_{\text{p}} F} \quad [11]$$

The above resistive film adds to the internal resistance of the anode, thereby negatively affecting battery performance

$$R_{\text{film}} = R_{\text{SEI}} + \frac{\delta_{\text{film}}}{K_{\text{p}}} \quad [12]$$

The above battery model suffers from two main numerical challenges. First, Eq. 3-8 create an algebraic loop within the model, thereby causing the model to have a nonzero index. This increases the computational cost of simulating the model considerably. Second, the fact that the spherical diffusion equation, Eq. 2, must be satisfied at every point in the anode and cathode creates a need for potentially very large numbers of state variables just for the purpose of calculating the solid concentration at every discretized point along the battery electrodes. The literature recognizes these two challenges and presents some methods for addressing them. The main contribution of this paper is its contribution of algebraic equation quasi-linearization and Padé approximation of spherical diffusion as two unique methods for addressing these challenges.

Quasi-Linearization Approach for Solving Algebraic Equations

Equations 3-8 in the above electrochemistry-based battery model form an algebraic loop. A consistent set of solutions to this algebraic loop must be obtained at every integration time step, which is essentially a root-finding problem. One may attempt to solve this problem using a number of different root-finding methods, including the Newton–Raphson method, fixed-point iteration, and optimization methods. These methods differ in numerical complexity and cost, but they all contribute significantly to the cost of simulating the full battery model numerically. This results in simulation speeds which are undesirable for system identification, optimization, and control studies. We therefore propose an alternative approach that significantly reduces the computational cost of solving the battery model's algebraic equations.

The proposed approach for solving the battery model's algebraic equations relies on two key insights. First, one can assume that the diffusion dynamics are much slower than the electrical dynamics. This allows one to freeze the equilibrium potentials U_{nref}, U_{pref} and solution conductivities K^{eff} and K_{D} in time (they still may vary spatially) when solving the algebraic equations. Now the only nonlinearities remaining in the algebraic equations are J_1 and J_{sd}. These are the Butler–Volmer (BV) expressions given in Eq. 3 and 10. Second, while the BV equation itself is nonlinear, this nonlinearity tends to produce very large changes in intercalation current densities for small increases in overpotential. This, in turn, generally forces the overpotentials to remain within some reasonable bounds over which the Butler–Volmer equation can be quasi-linearized. Quasi-linearization, in this context, is the process of linearizing the Butler–Volmer equation at every integration time step. This approximates the algebraic loop in the battery model by a different set of linear equations at every integration time step. The proposed approach results in a smaller Jacobian of only the algebraic equations, rather than the entire system of equations. So rather than having a square Jacobian with $(2/3) * M * N + (8/3) * \text{M}$ rows one has a square Jacobian with $(5/3) * M$ rows, where M is the number of points along the width of the cell and N is the number of points in the spherical direction. For the case $M = N = 100$, the proposed quasi-linearization approach furnishes a Jacobian matrix with 97.5% fewer rows than quasi-linearization of the entire system of model equations.

We now derive the quasi-linearization and then the block matrix form of the algebraic equations. This paper derives the case where all the anodic and cathodic transfer coefficients are equal, i.e., $\alpha = \alpha_{\text{an}} = \alpha_{\text{ap}} = \alpha_{\text{cn}} = \alpha_{\text{cp}}$. One can still perform the linearization if this is not the case. Equation 3 can be rewritten as

$$J_1 = 2 a_j i_{0,j} \sinh\left(\frac{\alpha F}{\bar{R} T} \eta_j \right) \quad [13]$$

This can be linearized about ϕ_1 and ϕ_2

$$J_1 = 2a_j i_{0,j}\left(\sinh\left(\frac{\alpha F}{\bar{R}T}\eta_j'\right) + \cosh\left(\frac{\alpha F}{\bar{R}T}\eta_j'\right)\frac{\alpha F}{\bar{R}T}((\phi_1 - \phi_1') - (\phi_2 - \phi_2'))\right) \quad [14]$$

where the primes denote the value associated with the point of the linearization. The equation for J_{sd} can be linearized as well

$$J_{sd} = i_{0,sd}a_n \exp\left(-\frac{\alpha F}{\bar{R}T}\eta_{sd}'\right)\left(\frac{\alpha F}{\bar{R}T}\right)((\phi_1 - \phi_1') - (\phi_2 - \phi_2')) \quad [15]$$

Now it is desirable to combine the linearization into the matrix equations related to the algebraic equations. These equations are derived by finite differencing Eq. 7 and 8 and including the 10 boundary value equations. First we define two diagonal matrices related to the linearizations

$$L_n[x,x] = \left(\frac{a_n\alpha F}{\bar{R}T}\right)\left(2i_{0n}\cosh\left(\frac{\alpha F}{\bar{R}T}\eta_n'(x)\right) + i_{0,sd}\exp\left(-\frac{\alpha F}{\bar{R}T}\eta_{sd}'(x)\right)\right) \quad [16]$$

$$L_p[x,x] = \left(\frac{a_p\alpha F}{\bar{R}T}\right)\left(2i_{0p}\cosh\left(\frac{\alpha F}{\bar{R}T}\eta_p'(x)\right)\right) \quad [17]$$

Now the block matrix form of the algebraic equations is

$$\begin{bmatrix} A_{1n}-L_n & 0 & L_n & 0 & 0 \\ 0 & A_{1p}-L_p & 0 & 0 & L_p \\ L_n & 0 & A_{2n}-L_n & 0 & 0 \\ 0 & 0 & 0 & A_{2s} & 0 \\ 0 & 0 & L_n & 0 & A_{2p}-L_p \\ \multicolumn{5}{c}{\text{Boundary Conditions}\ldots} \end{bmatrix}\begin{bmatrix}\phi_{1n}\\ \phi_{1p}\\ \phi_{2n}\\ \phi_{2s}\\ \phi_{2p}\end{bmatrix} = \begin{bmatrix} J_n' \\ J_p' \\ J_n' + F_n \\ F_s \\ J_p' + F_p \\ \text{BCs}\ldots \end{bmatrix} \quad [18]$$

where the A_1 matrices represent the $\nabla(\sigma^{eff}\nabla(\cdot))$ operator, A_2 matrices represent the $\nabla(K^{eff}\nabla(\cdot))$ operator, and the F vectors represent the $\nabla(K_D\nabla \ln(c_2))$ term. The J' vectors represent the value about which J has been linearized (recall that $J = J_1 + J_{sd}$). The last row in the block matrix equation consists of 10 equations representing the various boundary conditions.

The equation above is a system of linear equations and approximates the nonlinear algebraic equations. It is the result of freezing the diffusion dynamics and then linearizing the Butler–Volmer equation. Assuming that the nonlinear equations are solvable and that the integration time step of the model is small enough that the quasi-linearization remains "close enough" to the true value, this set of linear equations is solvable. Several numerical simulations (provided in a later section) indicate successful inversion and accurate solution of this matrix under various loading conditions. The numerical complexity of solving the equation depends on the number of discretization points along the electrodes and the separator. If N, S, and P indicate the number of points along anode, separator, and cathode, respectively, the associated matrix becomes a (sparse) square matrix of size $2N + S + 2P$. Although finer discretizations can improve the simulation accuracy, they may significantly increase simulation time.

In summary, the proposed quasi-linearization is accomplished by first freezing (in time) all state variables related to the diffusion dynamics and then linearizing the intercalation current equations, the only remaining nonlinearities. This furnishes three main computational benefits. First, the proposed approach improves the electrochemical model's tractability by greatly reducing the numerical difficulties involved in satisfying its algebraic equations. Second, the proposed quasi-linearization breaks the model's DAEs into two natural pieces, the differential equations and the algebraic equations, which can be solved in an alternative manner. Finally, the proposed quasi-linearization has a significant numerical speed advantage over quasi-linearizing the entire set of model equations, due to the smaller Jacobian.

A Family of Padé Approximations of Spherical Diffusion

This section examines the problem of reducing the order of the discretized Doyle–Fuller–Newman battery model using Padé approximations of Fick's law of spherical diffusion. The importance of these Padé approximations stems from the fact that spherical diffusion occur at every point across the width of the anode and cathode. If one creates M discretization points along the width of the battery cell, then roughly 2/3 of these points are in the anode and cathode (the rest would be in the separator). Furthermore, if one has N states in the spherical diffusion model then the total number of battery model states related to spherical diffusion is $(2/3)M * N$. Put another way, lowering the number of states in the spherical diffusion model by one lowers the number of states in the full model by $(2/3)M$. Thus the importance of reducing this submodel becomes clear.

The spherical diffusion model is a standard radially symmetric model governed by Fick's law. The input to this model is either intercalation current or intercalation current density, both of which impose Neumann (slope) boundary conditions. The paper handles both cases at once because they differ only by a multiple. The model's two outputs are volume-averaged total concentration $\bar{c}$ and surface concentration c_s. The total concentration $\bar{c}$ is related to battery SOC, and the surface concentration c_s affects the electrochemical reaction driving intercalation in the battery. The diffusion model governing these concentrations is a linear one-dimensional partial differential equation with one input and two outputs. It is given by

$$\frac{\partial c(t,R)}{\partial t} = D\left(\frac{\partial^2 c(t,r)}{\partial r^2} + \frac{2}{r}\frac{\partial c(t,r)}{\partial r}\right) \quad [19]$$

$$\frac{\partial c(t,R)}{\partial r} = -mu(t) \quad [20]$$

$$\begin{bmatrix} c_s \\ \bar{c} \end{bmatrix} = \begin{bmatrix} c(t,R) \\ \left(\dfrac{\int_0^R c(t,r)(4\pi r^2 dr)}{(4/3)\pi R^3}\right) \end{bmatrix} \quad [21]$$

where $c(t,r)$ is the concentration at time t and radial distance r (where $r = 0$ is the center and $r = R$ is the surface), D is the diffusion coefficient, u is either an intercalation current leaving the sphere or an intercalation current density leaving the sphere, m is a factor relating this to the boundary slope, c_s is the concentration at the surface of the sphere, $\bar{c}$ is the total concentration per volume, and R is the radius of the sphere.

One can compute transfer functions between the input and outputs by treating r as a parameter, i.e.

$$\mathcal{L}\left[\frac{\partial c(t,R)}{\partial t}\right] = \mathcal{L}\left[D\left(\frac{\partial^2 c(t,r)}{\partial r^2} + \frac{2}{r}\frac{\partial c(t,r)}{\partial r}\right)\right] \quad [22]$$

$$sC(s,r) = D\left(\frac{\partial^2 C(s,r)}{\partial r^2} + \frac{2}{r}\frac{\partial C(s,r)}{\partial r}\right) \quad [23]$$

Now consider the above one-dimensional boundary value problem with s as a parameter. This has the solution

$$C(s,r) = \frac{e^{\sqrt{s/D}(R-r)}(e^{2\sqrt{s/D}r} - 1)mR^2}{\left(1 + R\sqrt{\frac{s}{D}} + e^{2R\sqrt{s/D}}\left(R\sqrt{\frac{s}{D}} - 1\right)\right)r}U(s) \quad [24]$$

Equation 24 provides a transfer function from the input to an arbitrary radial distance in the sphere. Jacobsen and West have a study on impedance involving spherical diffusion that makes nice use of transfer functions.[19] Applying the (linear) evaluation operator $r = R$ yields the transfer function for c_s

$$\frac{C_s(s)}{U(s)} = -\frac{(e^{2R\sqrt{s/D}} - 1)mR}{1 + R\sqrt{\frac{s}{D}} + e^{2R\sqrt{s/D}}\left(R\sqrt{\frac{s}{D}} - 1\right)} \quad [25]$$

This is an infinite-dimensional transfer function with a countably infinite number of poles.

To evaluate the volume-averaged concentration, $\bar{c}$, one can use the following spherical integral

$$\frac{\bar{C}(s)}{U(s)} = \frac{\int_0^R C(s,r)(4\pi r^2 dr)}{(4/3)\pi R^3} = -\frac{3Dm}{Rs} \quad [26]$$

This spherical integral has canceled an infinite number of poles, leaving just a pure integrator. One need only integrate the input to compute $\bar{c}$ exactly. This makes physical sense if one considers a control volume around the sphere: one would only need to track what was going into and out of it to compute the total amount in the sphere. Because the averaged concentration transfer function is already quite simple in form we only need to make a Padé approximation for the surface concentration. This approximation is centered about zero due to the interest in lower frequency behavior.

The Padé approximation is a rational polynomial approximation to a function centered about a point. One can choose the desired order of the numerator P and denominator Q. The Padé approximation matches the value of the approximated function and all of its derivatives up to $(P + Q)$ terms at the centered point. One can compute the Padé approximation by directly enforcing these constraints. Padé approximations are commonly used for time delay transfer functions, which are also infinite-dimensional. Padé approximations are a good choice for approximating spherical diffusion because they can be centered about low frequency, handle infinite dimensionality without spatial discretization, are analytic, and can easily trade off speed versus accuracy by changing their order.

One slight modification to the standard Padé approximation is needed. Because the expansion is about zero and the function is undefined at zero (due to the removable pole at zero), first one multiplies by s and then computes the Padé approximation. After this we divide by s. This works because the pole at $s = 0$ is not an essential singularity. The order of the numerator is chosen one less than the order of the denominator, ensuring that the approximate transfer function is strictly proper.

The second-order Padé approximation for c_s will now be derived. The form of the Padé approximation is given in Eq. 27

$$P(s) = \frac{a_0 + a_1 s}{s(1 + b_2 s)} \quad [27]$$

First we multiply Eq. 25 by s, and then we evaluate this quantity at $s = 0$. Then the same is done for the first and second derivative. This same procedure is performed on the Padé approximation and the derivatives of equal order are equated

$$s\frac{C_s(s)}{U(s)}\bigg|_{s=0} = sP(s)|_{s=0} \Rightarrow -\frac{3dm}{R} = a_0 \quad [28]$$

$$\left(\frac{d}{ds}\left(s\frac{C_s(s)}{U(s)}\right)\right)\bigg|_{s=0} = \left(\frac{d}{ds}(sP(s))\right)\bigg|_{s=0} \Rightarrow -\frac{mR}{5} = a_1 - a_0 b_2 \quad [29]$$

$$\left(\frac{d^2}{ds^2}\left(s\frac{C_s(s)}{U(s)}\right)\right)\bigg|_{s=0} = \left(\frac{d^2}{ds^2}(sP(s))\right)\bigg|_{s=0} \Rightarrow \frac{2mR^3}{175} = 2b_2(-a_1 + a_0 b_2) \quad [30]$$

Solving these equations for a_0, a_1, and b_2, one finds the approximation given in Eq. 31

$$P(s) = -\frac{\frac{3dm}{R} + \frac{2mR}{7}s}{s + \frac{R^2}{35d}s^2} \quad [31]$$

The pole at origin in all of the Padé approximations can be used to compute $\bar{c}$ without increasing the number of states. One follows an identical method to derive higher order approximations. The second, third, and fourth-order approximations are tabulated in Table I.

Table I. Low-order padé approximations of C_s.

Order	padé approximation
Second	$\dfrac{-\frac{3dm}{R} - \frac{2mR}{7}s}{s + \frac{R^2}{35d}s^2}$
Third	$\dfrac{-\frac{3Dm}{R} - \frac{4mRs}{11} - \frac{mR^3s^2}{165D}}{s + \frac{3R^2s^2}{55D} + \frac{R^4s^3}{3465D^2}}$
Fourth	$\dfrac{-\frac{3Dm}{R} - \frac{2mRs}{5} - \frac{2mR^3s^2}{195D} - \frac{4mR^5s^3}{75075D^2}}{s + \frac{R^2s^2}{15D} + \frac{2R^4s^3}{2275D^2} + \frac{R^6s^4}{675675D^3}}$

The developed family of Padé approximations has several important characteristics. The family ranges from a one-state approximation to a countably infinite number of states, increasing in accuracy with the number of states. The approximations are generated through a systematic process with identical assumptions and all are analytical. The first few have been collected in Table I. The second to 10th-order Padé approximations compare well in the frequency domain to the true model (Fig. 1). The true model is given by the infinite-dimensional transfer function in Eq. 25. A comparison with finite differencing with 5 to 50 states in increments of 5 is shown Fig. 2, showing clearly that the Padé approximation provides much better accuracy per state.

Implementation of the Padé Approximates

This section demonstrates how to take the Padé approximation transfer function to a state space form for numerical simulation. Specifically, a set of state space equations is derived that computes both concentration at the surface and bulk concentration, without adding additional state variables. Then it is shown how one can

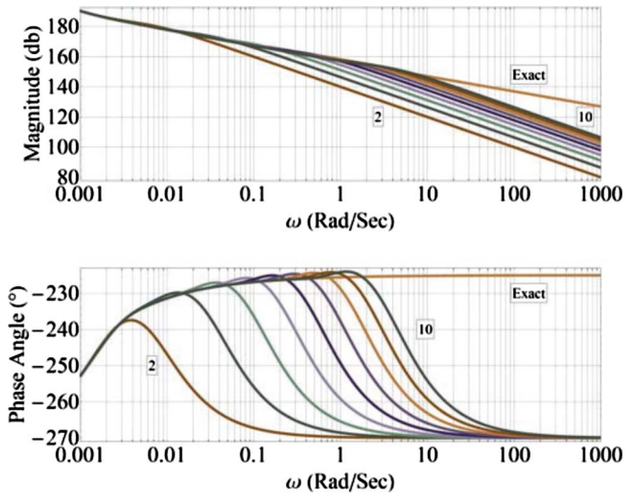

Figure 1. (Color online) Bode plot of C_s: padé approximation order 2 to 10 vs true model.

initialize a uniform concentration profile for this reduced model. These two steps create a model ready for numerical simulation.

One way to show that no additional state variables are needed to compute $\bar{c}$ is to consider the transfer function

$$\frac{C_s}{U}(s\,;\,Q) = \frac{a_0 + a_1 s + a_2 s^2 + \cdots + a_{Q-1}s^{Q-1}}{(1 + b_2 s + b_3 s^2 + \cdots + b_Q s^{Q-1})}\left(\frac{1}{s}\right) \quad [32]$$

where again Q is the order of the Padé approximation and U is (without loss of generality) either intercalation current or intercalation current density. This can be viewed as two transfer functions chained together

$$\frac{C_s}{\bar{C}}(s\,;\,Q) = \frac{a_0 + a_1 s + a_2 s^2 + \cdots + a_{Q-1}s^{Q-1}}{(1 + b_2 s + b_3 s^2 + \cdots + b_Q s^{Q-1})}\left(\frac{-R}{3Dm}\right) \quad [33]$$

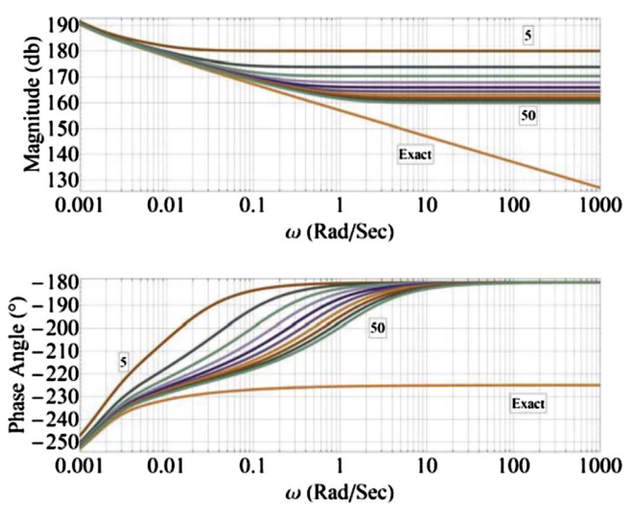

Figure 2. (Color online) Bode plot of C_s: finite difference method orders 5 to 50 in increments of 5 vs the true model.

$$\frac{\bar{C}}{U}(s) = -\frac{3Dm}{Rs} \quad [34]$$

where $\bar{c}$ is now an intermediate step in calculating c_s. This is due to $\bar{c}$ being an integrator and the transfer function from u to c_s having an integrator in it.

A (controllable canonical form) state space representation of this transfer function from u to c_s is

$$\dot{x} = \begin{bmatrix} 0 & 1 & 0 & 0 & \cdots & 0 \\ 0 & 0 & 1 & 0 & \cdots & 0 \\ 0 & 0 & 0 & \ddots & & 0 \\ \vdots & \vdots & \vdots & & 1 & 0 \\ 0 & 0 & 0 & 0 & 0 & 1 \\ 0 & \frac{1}{b_Q} & \frac{b_2}{b_Q} & \frac{b_3}{b_Q} & \cdots & \frac{b_{Q-1}}{b_Q} \end{bmatrix} x + \begin{bmatrix} 0 \\ \vdots \\ \vdots \\ \vdots \\ 0 \\ \frac{1}{b_Q} \end{bmatrix} u$$

$$c_s = [a_0 \quad a_1 \quad a_2 \quad \cdots \quad \cdots \quad a_{Q-1}]x \quad [35]$$

Now the pure integrator is located by canceling out all of the state variables' contribution in the A matrix

$$\dot{\bar{x}} = b_Q\left(\dot{x}_Q - \sum_{k=1}^{Q-1}\left(\frac{b_k}{b_Q}\dot{x}_k\right) + \frac{1}{b_Q}u\right) = u \quad [36]$$

Recall that $b_1 = 1$. Adding $\bar{c}$ as an output is accomplished by using the second row of the C matrix. The integrator scale factor is computed by noting that the surface concentration and total concentration per volume are equal under steady-state conditions

$$\bar{c} = -\left(\frac{a_0}{b_1}\right)[-b_1 \quad -b_2 \quad \cdots \quad -b_{Q-1} \quad b_Q]x \quad [37]$$

This brings the total system to

$$\dot{x} = \begin{bmatrix} 0 & 1 & 0 & 0 & \cdots & 0 \\ 0 & 0 & 1 & 0 & \cdots & 0 \\ 0 & 0 & 0 & \ddots & & 0 \\ \vdots & \vdots & \vdots & & 1 & 0 \\ 0 & 0 & 0 & 0 & 0 & 1 \\ 0 & \frac{1}{b_Q} & \frac{b_2}{b_Q} & \frac{b_3}{b_Q} & \cdots & \frac{b_{Q-1}}{b_Q} \end{bmatrix} x + \begin{bmatrix} 0 \\ \vdots \\ \vdots \\ \vdots \\ 0 \\ \frac{1}{b_Q} \end{bmatrix} u$$

$$y = \begin{bmatrix} c_s \\ \bar{c} \end{bmatrix} = \begin{bmatrix} a_0 & a_1 & a_2 & \cdots & a_{Q-1} \\ a_0 & a_0 b_2 & \cdots & a_0 b_{Q-1} & -a_0 b_Q \end{bmatrix} x \quad [38]$$

One common initialization for this model is that of uniform concentration profile. To do this one considers the constraints that a uniform concentration imposes and then finds x_0, the initial state variable vector to match these. The uniform concentration profile imposes three constraints: $\dot{x} = 0$, $c_s = \bar{c}$, and $u = 0$. The first constraint, $\dot{x} = 0$, leaves exactly one degree of freedom for x_0 because the A matrix's single zero eigenvalue gives it a kernel of dimension one. One can take the value of c_0, the height of the uniform concentration, and set $c_0 = c_s = \bar{c}$ and solve for the x_0. Due to the form of the zero eigenvalue's eigenvector, this reduces to

$$c_0 = [a_0 \quad a_1 \quad a_2 \quad \cdots \quad a_{Q-1}]\begin{pmatrix} x_{01} \\ 0 \\ \vdots \\ 0 \end{pmatrix} = a_0 x_{01} \quad [39]$$

The total concentration per volume will be automatically satisfied because the uniform profile requires it to equal the surface concentration. Initialization amounts to solving for x_{01} with Eq. 39 and setting the other elements of x_0 to zero.

Table II. Spherical diffusion parameters.

Parameter	Value
D (m^2/s)	2×10^{-16}
R (m)	1×10^{-6}
m (s/m^2)	1/D

This section has demonstrated how to take the Padé approximation transfer function to a state space form for numerical simulation. There were a few important subtleties in this process. First, even though the transfer function is between u and c_s one is able to compute $\bar{c}$ without adding any additional state variables. Second, a formula was given to initialize the concentration to a uniform profile. This was shown to depend on a single state variable. One can now take the state space form with the initialization and apply their choice of numerical simulation method.

Comparisons of Various Spherical Diffusion Approximations

The proposed Padé approximation is not the first attempt at reducing the spherical diffusion model. When constrained to using two or fewer states, the parabolic and quartic profile models are easy to implement and accurate at lower rates. When one has an idea of what signals will be fed into the model, POD is a good choice. For a specific frequency range, window residue grouping (RG) is very effective. Both POD and RG are numerical in nature. Padé approximation allows one to have an analytical method with an arbitrary number of states. This section presents comparisons in the frequency domain of the Padé approximation and various other approximations from the literature.

This paper does not nondimensionalize the spherical diffusion models because the main interest is how well they work inside the full battery model. A representative set of parameters is used for comparing the approximations. The parameters are given in Table II and are all identical to those in both Ref. 10 and 11. This makes the values in the Bode plots more physically meaningful.

While the single-input two-output spherical diffusion system has two transfer functions all the Bode plots are of c_s. Bode plots of $\bar{c}$ would not be enlightening because $\bar{c}$ is a pure integrator and every approximation with a zero eigenvalue will match it perfectly.

Parabolic and quartic profile approximations.— In Ref. 9, two ways of approximating spherical diffusion are considered. Both are based on approximating the spherical profile. One assumes a parabolic profile, and the other assumes a quartic profile. The surface concentration transfer functions for each are given in Eq. 40 and 41, respectively

$$\frac{C_s(s)}{U(s)} = -\frac{15mD - R^2ms}{5Rs} \quad [40]$$

$$\frac{C_s(s)}{U(s)} = -\frac{3150D^2m + 315DmR^2 + mR^4s^2}{35Rs(30D + R^2s)} \quad [41]$$

Bode plots of these along with the exact transfer function are presented in Fig. 3.

The parabolic profile has been shown to be effective in low rate battery simulation.[12] However it is not clear how to generalize this result to higher orders. The higher order polynomial which has two states slightly outperforms the second-order Padé approximation. This is due to the higher model having a direct input, whereas the Padé approximations are all strictly proper. Interestingly enough a non-strictly proper first-order Padé approximation is identical to the parabolic approximation.

POD approximation.— Reference 10 presents a POD-based model reduction of spherical diffusion. The Bode plot of this and Padé approximations 7th and 12th are given in Fig. 4.

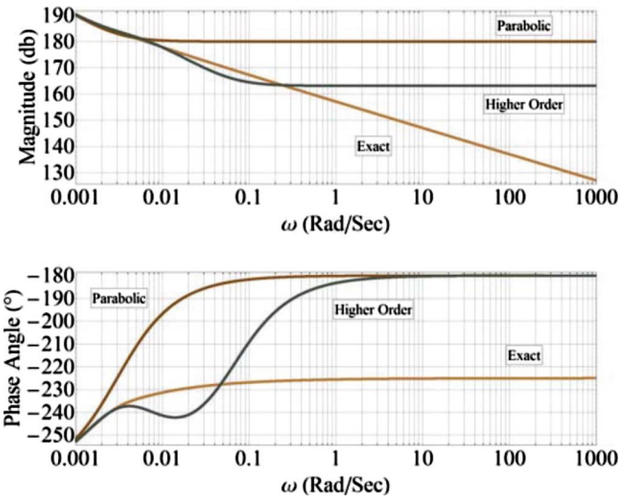

Figure 3. (Color online) Bode plot of C_s: the parabolic profile and quartic profile models vs the true model.

The approximation given in the paper is 12th order; a seventh-order Padé approximation exceeds its accuracy. The 12th order is given to compare the responses with an equal number of states. A major advantage of the POD method is that it allows the reconstruction of the entire state of the system, whereas the Padé approximation does not.

Residue grouping.— Residue grouping can also be used to reduce the diffusion models.[11] Instead of approximating the surface concentration, Ref. 11 approximates the difference of the surface concentration to the average concentration. Thus the correct steady-state behavior is zero, so there is no need to have a zero eigenvalue. This method focuses on matching the model in a specific frequency range. This is different from the Padé approximation as it matches steady state exactly and then extends toward faster frequencies. In moving from a Padé approximation to a residue grouping approximation one gives up some accuracy at lower frequencies, but in return one can get a good approximation for a wider frequency range. Figure 5 shows Padé approximations to the surface concentration minus the average concentration. The Bode plot is in hertz,

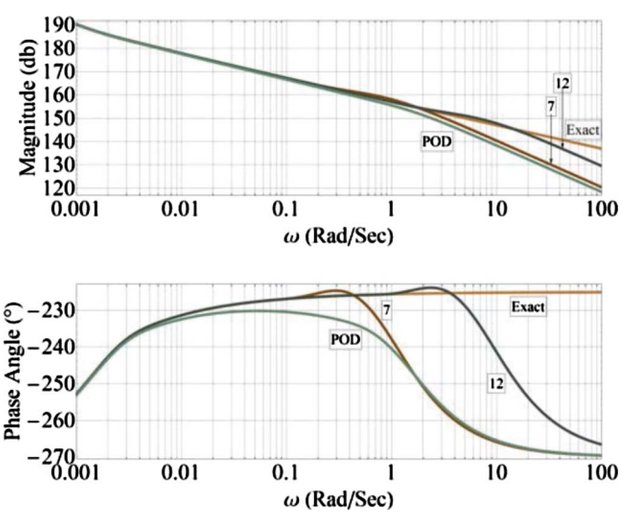

Figure 4. (Color online) Bode plot of C_s: pod, various Padé approximation, and the true model.

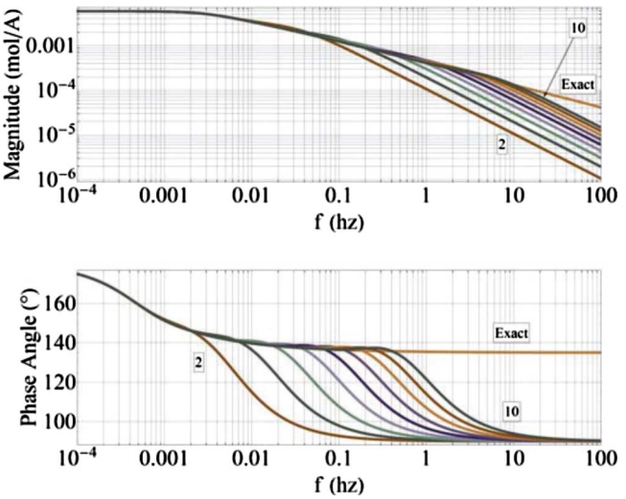

Figure 5. (Color online) Bode plot of C_s: Padé approximations 2 to 10 for comparison with Fig. 3, Ref. 11.

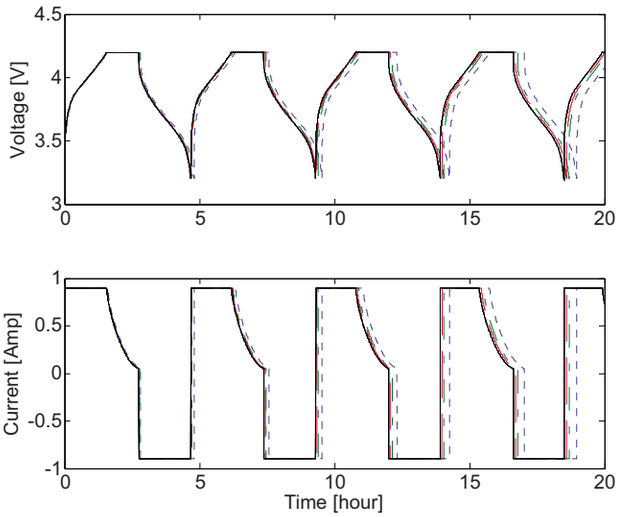

Figure 7. (Color online) Simulation of CCCV at 0.5C with various Padé approximations and finite differences.

and the magnitude values on the magnitude plot are absolute; this allows for direct comparison with Fig. 3 in Ref. 11.

Summary: Advantages of Padé approximation.— The family of Padé approximations is analytic, generalizable to any order, does not involve discretization, and preserves steady-state behavior. They compare favorably with finite differencing, parabolic and higher order polynomial approximations, and POD, although the Padé approximation does not allow for the reconstruction of the distribution. While Padé approximations are better than residue grouping at very low frequencies, residue grouping is an excellent method if one is concerned with a frequency window. The Padé approximation gives one an analytic option with an arbitrary number of states for reducing the model of spherical diffusion.

Numerical Simulations

Numerical simulation of the model with quasi-linearization and Padé approximation has been carried out to evaluate how the methods affect model accuracy and computational speed. Model parameters are identical to those in Ref. 7. Three different 20-h simulations of constant current constant voltage (CCCV) cycles were simulated at 0.1, 0.5, and 2.5C (0.18, 0.9, and 4.5A) with voltage limits of 3.1 and 4.2 V. All of the simulations used quasi-linearization.

While Padé approximation and finite difference both converge to accurate solutions, the Padé approximation converges at a much quicker rate with model order, as seen in Fig. 6-8. All of the Padé approximations give essentially identical battery simulation results, which implies that a second-order Padé approximation is sufficient at these C rates. One achieves very high accuracy with just a second-order Padé approximation, whereas one needs a 100th-order finite difference model for comparable results. Here one can reduce the number of state variables in each submodel by 98 and thus the full model by approximately $98 * (2/3) * M$ state variables. For $M = 100$ this results in a model with 6700 state variables decreasing to one with 134. This can lead to large increases in numerical performance. Simulation times are given in Table III for an implementation in MATLAB on a computer with a 2.0 GHz processor using 10 s time steps. While the 100th-order finite difference and second-

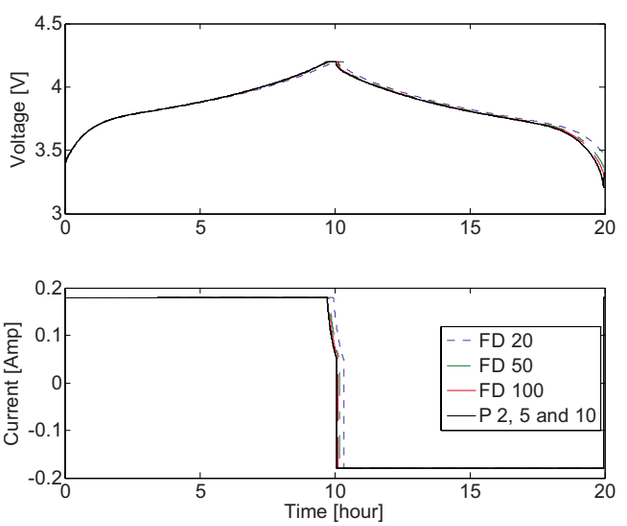

Figure 6. (Color online) Simulation of CCCV at 0.1C with various Padé approximations and finite differences.

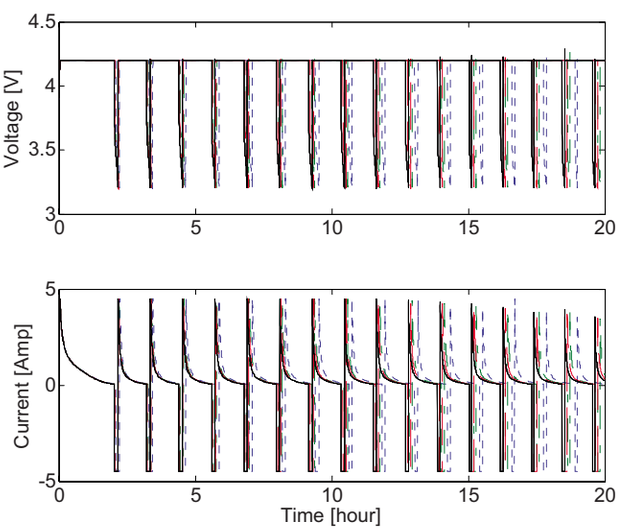

Figure 8. (Color online) Simulation of CCCV at 2.5C with various Padé approximations and finite differences.

Table III. Computational time in seconds for several 20-h CCCV simulations.

	FD 20	FD 50	FD 100	Padé 2	Padé 5	Padé 10
0.1 C	225.44	341.86	649.94	296.31	396.42	428.51
0.5 C	225.89	338.92	652.77	290.35	382.38	425.27
2.5 C	225.67	343.16	699.53	291.56	386.48	428.49

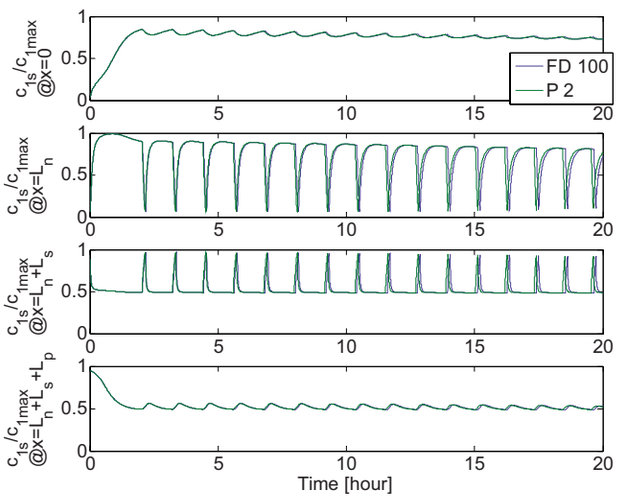

Figure 9. (Color online) Comparison Finite Difference 100 vs Padé 2 of $C_{1s}/C_{1\ max}$ at various interfaces in the cell for the 2.5C CCCV.

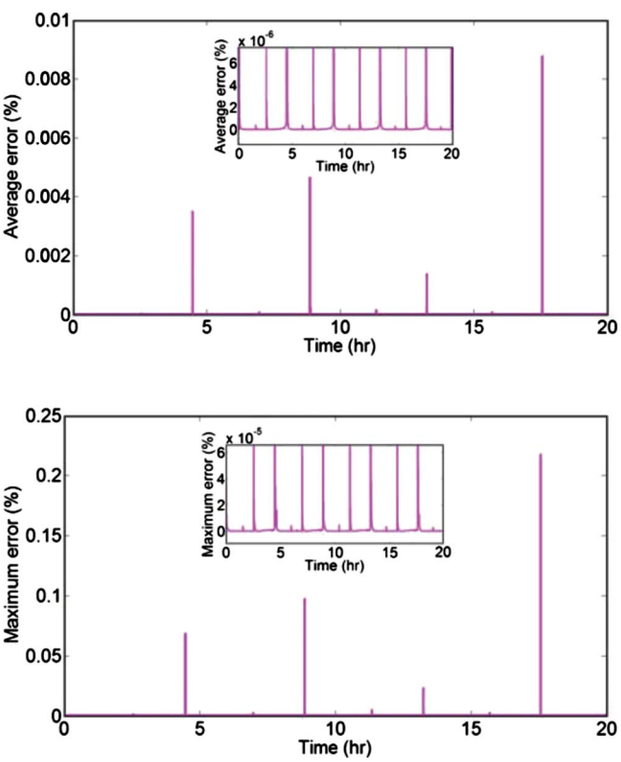

Figure 10. (Color online) Relative errors for CCCV at 0.5C; A Top: L^2 error of $J(x)$, Bottom: L^∞ error of $J(x)$.

order Padé approximation have comparable accuracy, the Padé approximation runs at least twice as quickly on all three cycles. Figure 9 shows the internal variable $c_{1s}/c_{1\max}$ at the boundaries and interfaces of the cell for a 100th-order finite difference and a second-order Padé approximation. This further reinforces the accuracy of the Padé approximation when used inside the full battery model.

Quasi-linearization is a highly accurate way to solve the nonlinear algebraic equations. The natural way to check this is to compute how accurately the quasi-linear solution satisfies the nonlinear algebraic equations. Because there is a large number of equations at each time step it is best to use two relative error norms to make sense of the data. The maximum relative error is given by an L^∞ norm in space and the average relative error is given by an L^1 norm in space. Figure 10 shows both of these error norms during the 0.5C CCCV simulation; the average error never exceeds 0.01% and the maximum error never exceeds 0.25%. In fact, for the vast majority of the time they are much lower. The spikes in these plots occur at abrupt changes in current. This is because the accuracy depends on how close the current linearization point is to the previous one and these are most different during these current changes.

It is difficult to determine how much faster quasi-linearization is over other methods because there is a vast number of methods for solving nonlinear equations. The quasi-linearization makes solving for the DAE's algebraic equations more efficient in two ways: it dramatically decreases the size of the Jacobian associated with the DAE and gives an analytical way to calculate it. It is the authors' experience that quasi-linearization is substantially faster than using optimization to solve the nonlinear algebraic equations. Applying both the Padé approximation and quasi-linearization greatly reduces the computational complexity of the model while maintaining very high accuracy.

Conclusion

Quasi-linearization and Padé approximation of diffusion substantially decrease the complexity and numerical cost of this electrochemical model. The quasi-linearization makes solving for the DAE's algebraic equations more efficient. The analytic Padé approximation of spherical diffusion greatly decreases the number of diffusion states in the model while remaining very accurate. These two contributions make using the Doyle, Fuller, and Newman model more tractable and conducive for optimization and control design.

Acknowledgments

The financial support of the NSF EFRI-RESIN program and the Michigan Public Service Commission is gratefully acknowledged. ASME has kindly granted permission for inclusion in this longer and more detailed article of Paper DSCC 2010–4084 by the same authors that was published in its proceedings.

University of Michigan assisted in meeting the publication costs of this article.

List of Symbols

a_j	specific area of the porous electrode j, 1/m
c_1	lithium concentration in the solid phase, mol/m^3
c_2	lithium concentration in the solution phase, mol/m^3
$c_{1,j}^{\max}$	maximum concentration of lithium in the sphere
$c_{1,j}^{s}$	lithium concentration at the surface of sphere
$D_{1,j}$	diffusion coefficient of lithium in the solid phase, m^2/s
D_2^{eff}	effective solution diffusion coefficient, m^2/s

F	Faraday's constant, C/mol
$i_{0,j}$	main intercalation reaction current density, A/m^2
$i_{0,\mathrm{sd}}$	side intercalation reaction current density, A/m^2
i_{app}	applied current density, A/m^2
J_1	main intercalation volumetric current density, A/m^3
J_{sd}	local volumetric current density for side reaction, A/m^3
K_{p}	film conductivity, 1/Ωm
k_j	rate constant of reaction, A/m^2 (mol/m^3)$^{1+\alpha}$
L	length of the cell, m
M_{p}	molecular weight of side reaction product, kg/mol
$\bar{R}$	universal gas constant, J/mol
R_{film}	film resistance at anode/solution interface, Ωm^2
R_{SEI}	film resistance due to solid electrolyte interface, Ωm^2
R	radius of sphere, m
T	temperature, K
t^+	transference number
$D_{\mathrm{ref},j}$	local equilibrium potential for main reaction, V
U_{sd}	local equilibrium potential for side reaction, V
α_{a}	anodic transfer coefficients of electrochemical reaction
α_{c}	cathodic transfer coefficients of electrochemical reaction
$\varepsilon_{1,j}$	volume fraction of electrode j
$\varepsilon_{2,j}$	volume fraction of solution
ϕ_1	local potential of solid, V
ϕ_2	local potential of solution, V
η_j	local over potential for main intercalation reaction, V
η_{sd}	local overpotential for side reaction, V
η_{sd}	effective conductivity of solution, S/m
κ^{eff}	effective conductivity of solution, S/m
κ_{D}	diffusional conductivity of solution, S/m
σ_j	conductivity of electrode, S/m
ρ_{p}	density of active material, kg/m^3
δ_{film}	resistive film thickness, m

Subscripts

n	anode/negative electrode
s	separator
p	cathode/positive electrode
j	*Solid*: $\forall j \in \{n,p\}$; *Solution*: $\forall j \in \{n,s,p\}$
1	solid
2	solution

Superscripts

eff	effective
max	maximum
S	surface

References

1. G. Plett, *J. Power Sources*, **134**, 252 (2004).
2. G. Plett, *J. Power Sources*, **134**, 262 (2004).
3. G. Plett, *J. Power Sources*, **134**, 277 (2004).
4. C. Speltino, D. Di Domenico, G. Fiengo, and A. Stefanopoulou, in *European Control Conference* (2009).
5. M. Doyle, T. Fuller, and J. Newman, *J. Electrochem. Soc.*, **140**, 1526 (1993).
6. T. Fuller, M. Doyle, and J. Newman, *J. Electrochem. Soc.*, **141**, 1 (1994).
7. P. Ramadass, B. Haran, P. Gomadam, R. White, and B. Popov, *J. Electrochem. Soc.*, **151**, A196 (2004).
8. M. Verbrugge, *J. Appl Electrochem*, **37**, 605 (2007).
9. V. Subramanian, V. Diwakar, and D. Tapriyal, *J. Electrochem. Soc.*, **152**, A2002 (2005).
10. L. Cai and R. White, *J. Electrochem. Soc.*, **156**, A154 (2009).
11. K. Smith, C. Rahn, and C. Wang, *J. Dyn. Syst., Meas., Control*, **130**, 1 (2008).
12. S. Santhanagopalan, Q. Guo, P. Ramadass, and R. White, *J. Power Sources*, **156**, 620 (2006).
13. V. Subramanian, V. Boovaragavan, and V. Diwakar, *Electrochem. Solid-State Lett.*, **10**, A255 (2007).
14. V. R. Subramanian, V. Boovaragavan V. Ramadesigan, and M. Arabandi, *J. Electrochem. Soc.*, **156**, A260 (2009).
15. V. Ramadesigan, V. Boovaragavan, J. Carl Pirkle, Jr., and V. R. Subramanian, *J. Electrochem. Soc.*, **157**, A854 (2010).
16. P. Arora, R. White, and M. Doyle, *J. Electrochem. Soc.*, **145**, 3647 (1998).
17. D. Aurbach, *J. Power Sources*, **89**, 206 (2000).
18. K. Smith and C. Wang, *J. Power Sources*, **161**, 628 (2006).
19. T. Jacobsen and K. West, *Electrochim. Acta*, **40** 255 (1995).